Title: Binucleated cells generated by nuclear movement during neural transdifferentiation from human bone marrow-derived mesenchymal cells

Authors: Carlos Bueno[1,*], Miguel Blanquer[1], David García-Bernal[1,2], Salvador Martínez[3] and José M. Moraleda[1].

[1]Medicine Department and Hematopoietic Transplant and Cellular Therapy Unit, Institute of Biomedical Research (IMIB), University of Murcia, Faculty of Medicine, Murcia, 30120, Spain.

[2]Biochemistry, Molecular Biology and Immunology Department, University of Murcia, Faculty of Medicine, Murcia, 30100, Spain

[3]Instituto de Neurociencias de Alicante (UMH-CSIC), Universidad Miguel Hernandez, San Juan, Alicante, 03550, Spain.

*Correspondence: Carlos Bueno, PhD., Medicine Department and Hematopoietic Transplant and Cellular Therapy Unit, Institute of Biomedical Research (IMIB), University of Murcia, Faculty of Medicine, Murcia, 30120, Spain. Tel.: 0034-968885013. Fax: 00-34-868884150. E-mail: carlos.bueno@um.es

Summary

Although it has been reported that bone marrow-derived mesenchymal stromal cells (BM-MSCs) can transdifferentiate into neural cells, the findings are considered unlikely. Cell changes induced by cytotoxicity and cell fusion events are alternative explanations for these observations in culture and transplantation studies, respectively. Here, we showed that BM-MSC neural transdifferentiation involves the formation of dedifferentiated cells which can then redifferentiate into neural-like cells, redifferentiate back to the mesenchymal fate or even repeatedly switch lineages without cell division. Furthermore, we have discovered that nuclei from dedifferentiated cells rapidly move within the cell, adopting different morphologies and even forming binucleated cells. We also noted that dedifferentiated cells position their nucleus at the front of the cell during migration. Our results demonstrated that BM-MSCs can rapidly transdifferentiate into neural-like cells and binucleated BM-MSCs can form with independence of any cell fusion events, suggesting that BM-MSC neural transdifferentiation is a fact, not an artifact.

Highlights

- hBM-MSC neural transdifferentiation involves the formation of dedifferentiated cells.
- hBM-MSCs could rapidly and repeatedly switch lineages without cell division.
- Nuclei from hBM-MSCs rapidly move within the cell adopting different morphologies.
- Binucleated hBM-MSCs can be formed with independence of any cell fusion events.

Introduction

We have known for many decades that adult cells can change their identity through dedifferentiation and transdifferentiation processes (Blau et al., 2001; Raff et al., 2003; Rajagopal et al., 2016). However, the cellular and molecular mechanisms that occur during these cell conversions are nuclear (Reid et al., 2018). It has been suggested that transdifferentiation may occur directly or it may involve a de-differentiation step before cells re-differentiation to a new mature phenotype. (Jopling et al., 2011; Merrell et al., 2016). Current research aims to understand the mechanisms of these these cell conversion processes and eventually harness them for use in regenerative medicine (Jopling et al., 2011; Eguizabal et al., 2013; Slack et al., 2007).

Several reports have indicated that mesenchymal stromal cells (MSCs) isolated from adult tissues can transdifferentiate into neural cells, both in vitro (Black et al., 2001; Woodbury et al., 2002; Muñoz-Elias et al., 2003; Jeong et al., 2004; Suon et al., 2004; Ning et al., 2016; Azedi et al., 2017; Radhakrishnan et al., 2019) and in vivo (Azizi et al., 1998; Kopen et al., 1999; Priller et al., 2001; Muñoz-Elias, G et al., 2004). However, the findings and their interpretation have been challenged (Krabbe et al., 2005; Kemp et al., 2014). The main argument against these observations in culture studies is that MSCs rapidly adopt neural-like morphologies through retraction of the cytoplasm, rather than by active neurite extension (Krabbe et al., 2005; Neuhuber et al., 2004; Lu et al., 2004). While transplantation studies have indicated that bone marrow-derived mesenchymal stromal cells (BM-MSCs) can contribute to the neuronal architecture of the nervous system, including Purkinje cells within the cerebellum (Azizi et al., 1998; Kopen et al., 1999; Priller et al., 2001; Muñoz-Elias, G., 2004., Kemp et al., 2014), the possibility of BM-MSCs transdifferenting into neural cells is considered unlikely, and the more accepted explanation that donor MSCs fuse with host

neurons (Kemp et al., 2014). Cell fusion has been put forward to explain the presence of gene-marked binucleated Purkinje neurons after gene-marked bone marrow-derived cell transplantation (Kemp et al., 2014; Alvarez-Dolado et al., 2003). We recently reported that MSCs isolated from adult human tissues (hMSCs) can transdifferentiate into neural-like cells without passing through a mitotic stage and that they shrank dramatically and changed their morphology to that of neural-like cells through active neurite extensión (Bueno et al., 2019; Bueno et al., 2021). These findings demonstrated that the transdifferentiation of hMSCs towards a neural lineage involves a dedifferentiation event prior to re-differentiation to neural phenotypes, thus definitively confirming that the rapid acquisition of a neural-like morphology during hMSC transdifferentiation is via a transdifferentiation trait rather than merely an artefact. Furthermore, we noted that nuclear remodelling occurred during in vitro neural transdifferentiation from hMSCs. We discovered that many hMSCs exhibit unusual nuclear structures and even possess two nuclei.

In the present study, we examined the sequence of biological events during neural transdifferentiation of human BM-MSCs (hBM-MSCs) by live-cell nucleus fluorescence labelling and time-lapse microscopy to determine whether the binucleation events observed during neural transdifferentiation from hMSCs are due to cell division or cell fusion events.

Results

Morphological changes in hBM-MSCs during neural transdifferentiation

We examined the sequence of biological events during neural transdifferentiation of histone H2B-GFP transfected hBM-MSCs by time-lapse microscopy. Time-lapse

imaging revealed that, after neural induction, hBM-MSCs can rapidly reshape from a flat to a spherical morphology. Subsequently, we observed that hMSC-derived round cells can maintain the spherical shape (Figure 1, green arrows; Movie S1) or assume new morphologies; round cells can change to a morphology similar to that of neural-like cells through active neurite extension (Figure 1, red arrows; Movie S1) or they can revert back to the mesenchymal morphology (Figure 1, yellow arrows; Movie S1).

The hBM-MSCs did not transdifferentiate at the same time or rate, so the cell culture simultaneously contained hBM-MSCs at different stages of transdifferentiation. Importantly, there was no cell proliferation or cell fusion through transdifferentiation from hBM-MSCs (Figure 1; Movie S1). These results confirm our previous findings (Bueno et al., 2013; Bueno et al., 2019; Bueno et al., 2021) and lend further support to the notion that MSCs transdifferentiate towards a neural lineage through a dedifferentiation step followed by re-differentiation to neural phenotypes.

As noted above, hBM-MSC-derived round cells can even preserve their spherical morphology for days without assuming new fates. However, it is important to note that cellular protrusions appeared, moved and disappeared from the surface of hBM-MSC-derived round cells during this dedifferentiation stage (Figure 2; Movie S2). Contrastingly, we also found that hBM-MSC-derived round cells can adopt a neural-like morphology via active neurite extension. (Figure 3; Movie S3). New neurites grew from the body of some round cells, which gradually adopted a more complex morphology, by acquiring dendrite-like (Figure 3, green arrows) and axon-like domains (Figure 3, yellow arrows). We did not observe any cellular protrusions as hBM-MSC-derived round cells gradually acquired a neural-like morphology. Finally, hBM-MSC-derived round and neural-like cells could also re-differentiate back to the mesenchymal morphology (Figures 1-3; Movies S1-S3). Surprisingly, hBM-MSCs could also rapidly

and repeatedly switch lineages without cell division (Figure 4; Movie S4). This finding is consistent with a previous study that report Schwann cells can undergo multiple cycles of differentiation and dedifferentiation without entering the cell cycle (Monje et al., 2010).

Nuclear remodelling during neural transdifferentiation from hBM-MSCs

Live-cell nucleus fluorescence labelling and time-lapse microscopy revealed that nuclear remodelling occurred during neural transdifferentiation from hBM-MSCs. Nuclei from histone H2B-GFP-expressing, hBM-MSC-derived round cells moved within the cell, adopting different morphologies and positions, and even forming lobed nuclei (Figure 5; Movie S5). Although the cell nuclei switched their morphologies while moving, the nuclear movement primarily produces three different nuclear morphologies and positions. Firstly, the cell nucleus acquired a finger-like shape and moves within the cell, generating the cellular protrusions that appeared and disappeared from the surface of hBM-MSC-derived round cells (Figure 6; Movie S6). Secondly, the nucleus acquired a finger-like shape, before reorienting towards a peripheral position within the cell and acquiring a kidney-like shape. Subsequently, the cell nucleus began to move rapidly around the cell (Figure S1; Movie S7). And thirdly, the nucleus acquired a finger-like shape and moved within the cell to form lobed nuclei connected by nucleoplasmic bridges. The lobed nuclei movement also generated transient cellular protrusions on the surface of hBM-MSC-derived round cells (Figure 7; Movie S8).

It is important to note that histone H2B-GFP-expressing, hBM-MSC-derived round cells position their nucleus at the front of the cell during migration (Figure S2; Movies S9 and S10). This nuclear positioning was observed in mononucleated hBM-MSC-derived round cells, in both cells with kidney shaped nuclei (Figure S2A; Movie S9) and cells with finger shaped nuclei (Figure S2B; Movie S10). hBM-MSC-derived round

cells with lobed nuclei also positioned their nucleus at the front of the cell during migration (Figure S3A; Movie S11). Furthermore, we observed that hBM-MSC-derived round cells with lobed nuclei positioned their largest lobe at the front of the cell during migration (Figure S3B; Movie S12). These finding are consistent with a previous study that reported that human leukocytes position their nucleus at the front of the cell during migration (Barzilai et al., 2010).

As mentioned previously, hBM-MSC-derived round cells can also assume new morphologies, gradually adopting a neural-like morphology through active neurite extension or re-differentiating back to their mesenchymal morphology. There were no changes in nuclear positioning or lobed nuclei formation as histone H2B-GFP-expressing, hBM-MSC-derived round cells gradually acquired a neural-like morphology (Figure S4; Movie S13). By contrast, when histone H2B-GFP-expressing, hBM-MSC-derived round cells reverted back to the mesenchymal morphology, the nuclei from mononucleated round cells gradually adopted their original ellipsoid shape (Figure S5A; Movie S14). Yet when round cells with lobed nuclei reverted back to the mesenchymal morphology, the lobed nuclei preserved their shape for hours (Figure S5B; Movie S15). In future studies, live-cell nucleus fluorescence labelling and time-lapse microscopy over longer periods is necessary to determine whether the lobed nuclei finally fused to form a single nucleus.

Finally, laser scanning confocal microscopy revealed that many histone H2B-GFP-expressing, hBM-MSC-derived round cells with unusual nuclear structures also exhibited extranuclear chromatin-containing bodies in the cellular cytoplasm during neural transdifferentiation (Figure S6). We observed that hBM-MSCs with finger shaped nuclei (Figure S6A), kidney shaped nuclei (Figure S6B) and lobed nuclei connected by nucleoplasmic bridges (Figure S6C) can also exhibit extranuclear bodies

in the cellular cytoplasm. Furthermore, we found chromatin-containing bodies connected to the main body of the nucleus by thin strands of nuclear material (Figure S6D), chromatin-containing bodies moving away from or toward the main nuclei (Figure S6E) and two lobed nuclei unconnected by any nucleoplasmic bridges with chromatin-containing bodies in the cellular cytoplasm (Figure S6F). These results indicate that binucleated hBM-MSCs form during neural transdifferentiation with independence of any cell division or fusion events.

Importantly, the nuclear morphology of hBM-MSCs observed during the transdifferentiation bears a lot of similarities to the nuclear morphology of neural stem cells located in the ventricular-subventricular zone of the anterolateral ventricle wall of the human foetal brain (Guerrero-Cázares et al., 2011) and adult mouse brain (Doetsch et al., 1997; Capilla-Gonzalez et al., 2014; Cebrián-Silla et al., 2017); their nuclear morphology is also very similar to that of many cultured hippocampal neurons (Wittmann et al., 2009). For example, the nuclear morphologies in Figure S6C are very similar to those observed in Wittmann et al. (2019, Fig. S2), Cebrián-Silla et al. (2017, Figs. 1E, 4I, 6F, S1B, S2B and S6A), Guerrero-Cázares et al. (2011, Fig. 2C) and Doetsch et al. (1997, Fig. 3A). Furthermore, the nuclear morphologies shown in Figure S6D closely resemble those reported by Cebrián-Silla et al. (2017, Figs. 1A,1B,1M,1N, 3I, 6A, 6B and 6H) and Guerrero-Cázares et al (2011, Fig. 3j). In addition, the nuclear morphologies in Figure S6E are very similar to those observed in Capilla-Gonzalez et al. (2014, Fig. S2C).

Discussion

In this study, we have shown that when hBM-MSCs were exposed to a neural induction medium, they rapidly reshaped from a flat to a spherical morphology. Subsequently,

hBM-MSC-derived round cells could preserve this the spherical morphology or assume new ones; they gradually adopted a neural-like morphology through active neurite extension or re-differentiated back to the mesenchymal fate. Furthermore, we found that hBM-MSCs can rapidly and repeatedly switch lineages without cell division. These results confirm our previous findings (Bueno et al., 2013; Bueno et al., 2019; Bueno et al., 2021) and further support the concept that transdifferentiation of MSCs towards a neural lineage occurs through a dedifferentiation step followed by re-differentiation to neural phenotypes.

This work also highlights that nuclear remodelling occurred during in vitro neural transdifferentiation from hMSCs. We discovered that nuclei in dedifferentiated cells rapidly moved within the cell, adopting different morphologies and even forming lobed nuclei. These nuclear movements generated transient cellular protrusions that appeared and disappeared from the surface of hBM-MSC-derived round cells. The dedifferentiated cells positioned their nucleus at the front of the cell during migration. These findings may suggest that nuclei in dedifferentiated cells are somehow sensing their surroundings. Future research is required to determine the feasibility of this conjecture.

This study not only shows that the main nuclei move within the cell, changing their morphology and position, but also that there are different sized chromatin-containing extranuclear bodies within cell cytoplasm. Therefore, it would be interesting to examine whether chromatin-containing bodies can move independently of the movement of the main nuclei or if they are a product of the main nuclei movement. In previous publications (Bueno et al., 2019; Bueno et al., 2021), we suggested that nuclear remodelling sequence might occur during neural transdifferentiation from hMSCs. Nevertheless, with new data, we have realised that this hypothesis was wrong because,

among other factors, it seems that not all hBM-MSCs form lobed nuclei during neural transdifferentiation. Future research is necessary to determine how nuclear remodelling occurs.

The literature published in recent decades has shown that MSCs isolated from adult tissues can form new neurons, both in culture (Black et al., 2001; Woodbury et al., 2002; Muñoz-Elias et al., 2003; Jeong et al., 2004; Suon et al., 2004; Ning et al., 2016; Azedi et al., 2017; Radhakrishnan et al., 2019) and transplantation studies (Azizi et al., 1998; Kopen et al., 1999; Priller et al., 2001; Muñoz-Elias, G et al., 2004). However, the findings and their interpretations have been challenged (Krabbe et al., 2005; Kemp et al., 2014). It has been argued that the rapid neural transdifferentiation of MSCs reported in culture studies is actually due to cytotoxic changes induced by the media (Krabbe et al., 2005; Neuhuber et al., 2004; Lu et al., 2004), so the rapid changes should not be interpreted as signs of transdifferentiation. While transplantation studies indicated that BM-MSCs can contribute to the neuronal architecture of the central nervous system, including that of Purkinje cells within the cerebellum (Azizi et al., 1998; Kopen et al., 1999; Priller et al., 2001; Muñoz-Elias, et al., 2004., Kemp et al., 2014), it remains unclear whether the underlying mechanism is transdifferentiation or BM-MSC-derived cell fusion with the existing neuronal cells, or both (Kemp et al., 2014). Cell fusion has been put forward to explain the presence of gene-marked binucleated Purkinje neurons after gene-marked bone marrow-derived cell transplantation (Kemp et al., 2014; Alvarez-Dolado et al., 2003). In this study, we have shown that BM-MSCs can rapidly adopt a neural-like morphology through active neurite extension. Furthermore, we demonstrated that binucleated hBM-MSCs can be formed during neuronal transdifferentiation with independence of any cell fusion

events. Therefore, our results provide futher evidence that MSCs isolated from adult tissues can overcome their mesenchymal fate and transdifferentiate into neural cells.

Importantly, the nuclear morphology of hBM-MSCs observed during the transdifferentiation bears a lot of similarities to the nuclear morphology of neural stem cells located in the ventricular-subventricular zone of the anterolateral ventricle wall of the human foetal brain (Guerrero-Cázares et al., 2011) and adult mouse brain (Doetsch et al., 1997; Capilla-Gonzalez et al., 2014; Cebrián-Silla et al., 2017); their nuclear morphology is also very similar to that of many cultured hippocampal neurons (Wittmann et al., 2009). Although it has generally been believed that adult neurogenesis occurs progressively through sequential phases of proliferation and neuronal differentiation of adult stem cells (Bond et al., 2015), the approaches used to probe stem cell division and differentiation, and even direct lineage tracing, are inherently limited (Rakic et al., 2002; Cooper-Kuhn et al., 2002; Breunig et al., 2007; Kuhn et al., 2016; Sorrells et al., 2021). What is more, many authors have reported binucleated neurons in various central and peripheral parts of the nervous system including, the hippocampus (Altman et al., 1963), cerebellum (Magrassi et al., 2007; Das et al., 1977), sympathetic and spinal ganglia (Das et al., 1977), cerebral cortex (Das et al., 1977) and spinal cord (Das et al., 1977). Collectively, these findings suggest that new neurons can also be generated without necessitating cell division. Future research is required to determine the likelihood of this premise.

In conclusion, our results indicate that BM-MSC neural transdifferentiation is a fact and not an artifact. Therefore, hMSCs can be used to understand how cellular conversion processes work (Reid et al., 2018; Jopling et al., 2011; Merrell et al., 2016) and to eventually harness them for use in the treatment of neurological disorders (Choudhary et al., 2021).

Experimental procedures

Ethical conduct of research

The authors declare that all protocols used to obtain and process all human samples were approved by the local ethics committees (UMH.IN.SM.03.16, HULP3617.05/07/2012 and HUSA19/1531.17/02/2020) according to Spanish and European legislation and conformed to the ethical guidelines of the Helsinki Declaration. Donors provided written informed consent before obtaining samples.

Isolation and culture of hBMSCs

Bone marrow aspirates were obtained by percutaneous direct aspiration from the iliac crest of 5 healthy volunteers at University Hospital Virgen de la Arrixaca (Murcia, Spain). Bone marrow was collected with 20 U/ml sodium heparin, followed by a Ficoll density gradient-based separation by centrifugation at 540g for 20 min. After, mononuclear cell fraction was collected, washed twice with Ca^{2+}/Mg^{2+}-free phosphate buffered saline (PBS) (Gibco Invitrogen) and seeded into 175-cm2 culture flasks (Nunc, Thermo Fisher Scientific) at a cell density $1.5x10^5$ cells/cm^2 in serum-containing media (designated as the basal media), composed of DMEM low glucose medium (Thermo Fisher Scientific) supplemented with 10% fetal bovine serum (FBS; Lonza), 1% GlutaMAX (Thermo Fisher Scientific), non-essential amino acid solution (Sigma-Aldrich) and 1% penicillin/streptomycin (Thermo Fisher Scientific). After 3 days of culture at 37ºC and 7% CO_2, non-attached cells were removed and fresh complete medium was added. Culture media were renewed every 2 days, and the isolated hBMSCs were passaged when cultures were 70-80% confluent. All studies were performed using hBMSCs expanded within culture passages 3-4.

Expression Vectors and Cell Transfection

The expression vectors used in the present study were H2B-eGFP, a gift from Geoff Wahl (Addgene plasmid # 11680; http://n2t.net/addgene:11680; RRID:Addgene_11680; Kanda et al., 1998). Isolated hBMSCs-derived cells were transfected using the Gene Pulser-II Electroporation System (Bio-Rad Laboratories). Electroporation was performed in a sterile cuvette with a 0.4-cm electrode gap (Bio-Rad Laboratories), using a single pulse of 270 V, 500 μF. Plasmid DNA (5 μg) was added to 1.5×10^6 viable hBMSCs-derived cells in 0.2-ml DMEM low glucose medium (Thermo Fisher Scientific) before electrical pulsing.

Time-lapse microscopy of histone H2B-GFP expressing hBM-MSCs cultured in neural induction media

We used μ-Dish 35 mm, high Grid- 500 (Ibidi) for live cell imaging. Histone H2B-GFP transfected hBM-MSCs were plated onto collagen IV (Sigma-Aldrich) coated plastic or glass coverslips. To induce neural differentiation, cells at passage 3–4 were allowed to adhere to the plates overnight. Basal media was removed the following day and the cells were cultured for 2 days in serum-free media (designated as the neural basal media) consisting in Dulbecco's modified Eagle's medium/F12 (DMEM/F12 Glutamax, Gibco) supplemented with N2-supplement (R&D systems), 0.6% glucose (Sigma-Aldrich), 5mM HEPES (Sigma-Aldrich), 0.5% human serum albumin (Sigma-Aldrich), 0.0002% heparin (Sigma-Aldrich), non-essential amino acid solution (Sigma-Aldrich) and 100 U/ml penicillin-streptomycin (Sigma-Aldrich). On day 3, cells were cultured in neural induction media, consisting in the neural basal media supplemented with 500nM retinoic acid (Sigma-Aldrich), 1mM dibutyryl cAMP (Sigma-Aldrich) and the growth factors BDNF (10□ng/ml; Peprotech), GDNF (10□ng/ml; Peprotech) and IGF-1 (10□ng/ml; R&D systems). Time-lapse analysis was carried out using a Widefield

Leica Thunder-TIRF imager microscope. We perform time-lapse microscopy within the first 71 hr after neural induction media was added directly to the cells. Time-lapse images were obtained every 30 min. During imaging, cells were enclosed in a chamber maintained at 37°C under a humidified atmosphere of 5% CO2 in air. Data are representative of ten independent experiments.

Immunocytochemistry

A standard immunocytochemical protocol was used as previously described (Bueno et al., 2013; Bueno et al., 2019; Bueno et al., 2021). Histone H2B-GFP transfected hBM-MSCs were plated onto collagen IV (Sigma-Aldrich) coated plastic or glass coverslips and maintained in neural induction media. Cells were rinsed with PBS and fixed in freshly prepared 4% paraformaldehyde (PFA; Sigma-Aldrich). Fixed cells were blocked for 2 h in PBS containing 10% normal horse serum (Gibco) and 0.25% Triton X-100 (Sigma) and incubated overnight at 4 °C with antibodies against β-III-tubulin (TUJ1; 1:500, Covance) in PBS containing 1% normal horse serum and 0.25% Triton X-100. On the next day, cells were rinsed and incubated with the secondary antibody conjugated with Alexa Fluor® 594 (anti-mouse; 1:500, Molecular Probes). Cell nuclei were counterstained with DAPI (0.2 mg/ml in PBS, Molecular Probes).

Images and Data Analyses

Photograph of visible and fluorescent stained samples were carried out in a Widefield Leica Thunder-TIRF imager microscope equipped with a digital camera or in confocal laser scanning microscope Leica TCS-SP8. We used Filmora Video Editor software for video editing and Photoshop software to improve the visibility of fluorescence images without altering the underlying data.

Acknowledgements: We greatly appreciate the technical assistance of Microscopy Section and the Tissue Culture Service of the University of Murcia.

Author contributions: C.B. conceived of the study, designed the study, carried out the molecular lab work and drafted the manuscript; M.B. and D.G-B. designed experiments, participated in data analysis and helped draft the manuscript; S.M. and J.M.M. helped draft the manuscript and financial support.

Declaration of interests: The authors declare no competing interests.

Funding: This study was supported by the Spanish Ministry of Science and Innovation, the Carlos III Health Institute (ISCIII), through the Spanish Network of Cell Therapy (TerCel), RETICS subprogram, projects RD16/0011/0001 and RD16/0011/0010, co-funded by European Regional Development Fund (ERDF) "Una manera de hacer Europa". It was also partially supported by MINECO/AEI/ERDF, EU, Spanish Ministry of Economy, Industry and Competitiveness, the Spanish State Research Agency and the European Union through the ERDF– "Una manera de hacer Europa" (proyect SAF2017-83702-R); The Generalitat Valenciana (Prometeo/2018/041); Research Grant of the Universidad Católica San Antonio de Murcia (UCAM).

References

Alvarez-Dolado, M., Pardal, R., Garcia-Verdugo, J.M., Fike, J.R., Lee, H.O., Pfeffer, K., Lois, C., Morrison, S.J., and Alvarez-Buylla, A. (2003). Fusion of bone-marrow-derived cells with Purkinje neurons, cardiomyocytes and hepatocytes. Nature *425*, 968-973. 10.1038/nature02069.

363 Altman, J. (1963). Autoradiographic investigation of cell proliferation in the brains of
364 rats and cats. Anat. Rec. *145*, 573-591. 10.1002/ar.1091450409.

365 Azedi, F., Kazemnejad, S., Zarnani, A.H., Soleimani, M., Shojaei, A., and Arasteh, S.
366 (2017). Comparative capability of menstrual blood versus bone marrow derived stem
367 cells in neural differentiation. Mol. Biol. Rep. *44*, 169–182. 10.1007/s11033-016-4095-
368 7.

369 Azizi, A.S., Stokes, D., Augelli, B.J., DiGirolamo, C., and Prockop, D.J. (1998).
370 Engraftment and migration of human bone marrow stromal cells implanted in the brains
371 of albino rats – similarities to astrocyte grafts. Proc. Natl. Acad. Sci. U S A *95*, 3908-
372 3913. 10.1073/pnas.95.7.3908.

373 Barzilai, S., Yadav, S.K., Morrell, S., Roncato, F., Klein, E., Stoler-Barak, L., Golani,
374 O., Feigelson, S.W., Zemel, A., Nourshargh, S., et al. (2017). Leukocytes Breach
375 Endothelial Barriers by Insertion of Nuclear Lobes and Disassembly of Endothelial
376 Actin Filaments. Cell Rep. *18*, 685-699. 10.1016/j.celrep.2016.12.076.

377 Black, I.B., and Woodbury, D. (2001). Adult rat and human bone marrow stromal stem
378 cells differentiate into neurons. Blood Cells Mol. Dis. *27*, 632-636.
379 10.1006/bcmd.2001.0423.

380 Blau, H.M., Brazelton, T.H., and Weimann, J.M. (2001). The evolving concept of a
381 stem cell: entity or function? Cell *105*, 829-841. 10.1016/s0092-8674(01)00409-3.

382 Bond, A. M., Ming, G.L., and Song, H. (2015). Adult mammalian neural stem cells and
383 neurogenesis: five decades later. Cell Stem Cell *17*, 385–395.
384 10.1016/j.stem.2015.09.003.

385 Breunig, J.J., Arellano, J.I., Macklis, J.D., and Rakic, P. (2007). Everything that glitters
386 isn't gold: a critical review of postnatal neural precursor analyses. Cell Stem Cell *1*,
387 612–627. 10.1016/j.stem.2007.11.008.

388 Bueno, C., Ramirez, C., Rodríguez-Lozano, F.J, Tabarés-Seisdedos, R., Rodenas, M.,
389 Moraleda, J.M., Jones, J.R., and Martinez, S. (2013). Human adult periodontal
390 ligament-derived cells integrate and differentiate after implantation into the adult
391 mammalian brain. Cell Transplant. *22*, 2017–2028. 10.3727/096368912X657305.

392 Bueno, C., Martínez-Morga, M., and Martínez, S. (2019). Non-proliferative
393 neurogenesis in human periodontal ligament stem cells. Sci. Rep. *9*, 18038.
394 101038/s41598-019-54745-3.

395 Bueno, C., Martínez-Morga, M., García-Bernal, D., Moraleda, J.M., and Martínez, S.
396 (2021). Differentiation of human adult-derived stem cells towards a neural lineage
397 involves a dedifferentiation event prior to differentiation to neural phenotypes. Sci Rep.
398 *11*, 12034. 10.1038/s41598-021-91566-9.

399 Capilla-Gonzalez, V., Cebrian-Silla, A., Guerrero-Cazares, H., Garcia-Verdugo, J.M.
400 and Quiñones-Hinojosa, A. (2014). Age-related changes in astrocytic and ependymal
401 cells of the subventricular zone. Glia *62*, 790–803. 10.1002/glia.22642.

402 Cebrián-Silla, A., Alfaro-Cervelló, C., Herranz-Pérez, V., Kaneko, N., Park, D.H,
403 Sawamoto, K., Alvarez-Buylla, A., Lim, D.A., and García-Verdugo, J.M. (2017).
404 Unique organization of the nuclear envelope in the post-natal quiescent neural stem
405 cells. Stem Cell Reports *9*, 203–216. 10.1016/j.stemcr.2017.05.024.

406 Choudhary, P., Gupta, A., and Singh, S. (2021). Therapeutic Advancement in Neuronal
407 Transdifferentiation of Mesenchymal Stromal Cells for Neurological Disorders. J. Mol.
408 Neurosci. *7*, 889-901. 10.1007/s12031-020-01714-5.

409 Cooper-Kuhn, C.M., and Kuhn, H.G. Is it all DNA repair? (2002). Methodological
410 considerations for detecting neurogenesis in the adult brain. Brain Res. Dev *134*, 13–21.
411 0.1016/s0165-3806(01)00243-7.

412 Das, G.D. (1977). Binucleated neurons in the central nervous system of the laboratory
413 animals. Experientia *33*, 1179-80. 10.1007/BF01922313.

414 Doetsch, F., Garcia-verdugo, J.M., and Alvarez-buylla, A. (1997). Cellular composition
415 and three-dimensional organization of the subventricular germinal zone in the adult
416 mammalian brain. J. Neurosci. *17*, 5046–5061. 10.1523/JNEUROSCI.17-13-
417 05046.1997.

418 Eguizabal, C., Montserrat, N., Veiga, A., and Izpisua Belmonte J.C. (2013).
419 Dedifferentiation, transdifferentiation, and reprogramming: future directions in
420 regenerative medicine. Semin. Reprod. Med. *31*, 82-94. 10.1055/s-0032-1331802.

421 Guerrero-Cázares, H., Gonzalez-Perez, O., Soriano-Navarro, M., Zamora-Berridi, G.,
422 García-Verdugo, J.M., and Quinoñes-Hinojosa, A. (2011). Cytoarchitecture of the
423 lateral ganglionic eminence and rostral extension of the lateral ventricle in the human
424 fetal brain. J. Comp. Neurol. *519*, 1165–1180. 10.1002/cne.22566.

425 Jeong, J.A., Gang, E.J., Hong, S.H., Hwang, S.H., Kim, S.W., Yang, I.H., Ahn, C.,
426 Han,H., and Kim, H. (2004). Rapid neural differentiation of human cord blood-derived
427 mesenchymal stem cells. Neuroreport *15*, 1731–1734.
428 10.1097/01.wnr.0000134846.79002.5c.

429 Jopling, C., Boue, S., and Izpisua Belmonte J.C. (2011). Dedifferentiation,
430 transdifferentiation and reprogramming: three routes to regeneration. Nat. Rev. Mol.
431 Cell Biol. *12*, 79-89. 10.1038/nrm3043.

Kanda, T., Sullivan, K.F., and Wahl, G.M. (1998). Histone-GFP fusion protein enables sensitive analysis of chromosome dynamics in living mammalian cells. Curr. Biol. *8*, 377-385. 10.1016/s0960-9822(98)70156-3.

Kemp, K., Wilkins, A., and Scolding, N. (2014). Cell fusion in the brain: two cells forward, one cell back. Acta Neuropathol. *128*, 629-38. 10.1007/s00401-014-1303-1.

Kopen, G.C., Prockop, D.J., and Phinney, D.G. (1999). Marrow stromal cells migrate throughout forebrain and cerebellum, and they differentiate into astrocytes after injection into neonatal mouse brains. Proc. Natl. Acad. Sci. USA *96*, 10711–10716. 10.1073/pnas.96.19.10711.

Kuhn, H.G., Eisch, A.J., Spalding, K., and Peterson, D.A. (2016). Detection and Phenotypic Characterization of Adult. Neurogenesis. Cold Spring Harb. Perspect. Biol. *8*, a025981. 10.1101/cshperspect.a025981.

Krabbe, C., Zimmer, J., and Meyer, M. (2005). Neural transdifferentiation of mesenchymal stem cells - a critical review. APMIS *113*, 831–844. 10.1111/j.1600-0463.2005.apm_3061.x.

Lu, P., Blesch, A., and Tuszynski, M.H. (2004). Induction of bone marrow stromal cells to neurons: differentiation, transdifferentiation, or artifact? J. Neurosci. Res. **77**, 174-191. 10.1002/jnr.20148.

Magrassi, L., Grimaldi, P., Ibatici A., Corselli, M., Ciardelli, L., Castello, S., Podestà, M., Frassoni, F., and Rossi, F. (2007). Induction and survival of binucleated Purkinje neurons by selective damage and aging. J. Neurosci. *27*, 9885-9892. 10.1523/JNEUROSCI.2539-07.2007.

454 Merrell, A.J., and Stanger, B.Z. (2016). Adult cell plasticity in vivo: de-differentiation
455 and transdifferentiation are back in style. Nat. Rev. Mol. Cell Biol. *17*, 413-25.
456 10.1038/nrm.2016.24.

457 Monje, P.V., Soto, J., Bacallao, K., and Wood, P.M. (2010). Schwann cell
458 dedifferentiation is independent of mitogenic signaling and uncoupled to proliferation:
459 role of cAMP and JNK in the maintenance of the differentiated state. J. Biol. Chem.
460 *285*, 31024-31036. 10.1074/jbc.M110.116970.

461 Muñoz-Elias, G., Marcus, A.J., Coyne, T.M., Woodbury, D., and Black, I.B. (2004).
462 Adult bone marrow stromal cells in the embryonic brain: engraftment, migration,
463 differentiation, differentiation, and long-term survival. J. Neurosci. *24*, 4585-4595.
464 10.1523/JNEUROSCI.5060-03.2004.

465 Muñoz-Elias, G., Woodbury, D., and Black, I.B. (2003). Marrow stromal cells, mitosis
466 and neuronal differentiation: stem cell and precursor functions. Stem Cells *21*,437–448.
467 10.1634/stemcells.21-4-437.

468 Neuhuber, B., Gallo, G., Howard, L., Kostura, L., Mackay, A., and Fischer, I. (2004).
469 Reevaluation of in vitro differentiation protocols for bone marrow stromal cells:
470 disruption of actin cytoskeleton induces rapid morphological changes and mimics
471 neuronal phenotype. J. Neurosci. Res. *77*, 192-204. 10.1002/jnr.20147.

472 Ning, H., Lin, G., Lue, T.F., and Lin, C.S. (2016). Neuron-like differentiation of adipose
473 tissue-derived stromal cells and vascular smooth muscle cells. Differentiation *74*, 510-
474 518. 10.1111/j.1432-0436.2006.00081.x.

475 Priller, J., Persons, D.A., Klett, F.F., Kempermann, G., Kreutzberg, G.W., and Dirnagl,
476 U. (2001). Neogenesis of cerebellar Purkinje neurons from gene-marked bone marrow
477 cells in vivo. J. Cell Biol. *155*, 733-738. 10.1083/jcb.200105103.

478 Radhakrishnan, S., Trentz, O.A., Reddy, M.S., Rela, M., Kandasamy, M., and
479 Sellathamby, S. (2019). In vitro transdifferentiation of human adipose tissue-derived
480 stem cells to neural lineage cells - a stage-specific incidence. Adipocyte *8*, 164–177.
481 10.1080/21623945.2019.1607424.

482 Raff, M. Adult stem cell plasticity: fact or artifact? (2003). Annu. Rev. Cell Dev. Biol.
483 *19*, 1-22. 10.1146/annurev.cellbio.19.111301.143037.

484 Rajagopal, J., and Stanger B.Z. (2016). Plasticity in the Adult: How Should the
485 Waddington Diagram Be Applied to Regenerating Tissues? Dev. Cell *36*, 133-137.
486 10.1016/j.devcel.2015.12.021.

487 Rakic, P. (2002). Adult neurogenesis in mammals: an identity crisis. J. Neurosci. *22*,
488 614–618. 10.1523/JNEUROSCI.22-03-00614.2002.

489 Reid, A., and Tursun, B. (2018). Transdifferentiation: do transition states lie on the path
490 of development? Curr. Opin. Syst. Biol. *11*, 18-23. 10.1016/j.coisb.2018.07.004.

491 Slack, J.M. (2007). Metaplasia and transdifferentiation: from pure biology to the clinic.
492 Nat Rev Mol. Cell Biol. *8*, 369-78. 10.1038/nrm2146.

493 Sorrells, S.F., Paredes, M.F., Zhang, Z., Kang, G., Pastor-Alonso, O., Biagiotti, S.,
494 Page, C.E., Sandoval, K., Knox, A., Connolly, A., et al. (2021). Positive controls in
495 adults and children support that very few, if any, new neurons are born in the adult
496 human hippocampus. J. Neurosci. *41*, 2554–2565. 10.1523/JNEUROSCI.0676-20.2020.

497 Suon, S., Jin, H., Donaldson, A.E., Caterson, E.J., Tuan, R.S., Deschennes, G.,
498 Marshall, C., and Iacovitti, L. (2004). Transient differentiation of adult human bone
499 marrow cells into neuron-like cells in culture: development of morphological and

biochemical traits is mediated by different molecular mechanisms. Stem Cells Dev. *13*, 625-635. 10.1089/scd.2004.13.625.

Wittmann, M., Queisser, G., Eder, A., Wiegert, J.S., Bengtson, C.P., Hellwig, A., Wittum, G., and Bading, H. (2009). Synaptic activity induces dramatic changes in the geometry of the cell nucleus: interplay between nuclear structure, histone H3 phosphorylation, and nuclear calcium signaling. J. Neurosci. *29*, 14687–14700. 10.1523/JNEUROSCI.1160-09.2009.

Woodbury, D., Reynolds, K., and Black, I.B. (2002). Adult bone marrow stromal stem cells express germline, ectodermal, endodermal, and mesodermal genes prior to neurogenesis. J. Neurosci. Res *69*, 908-917. 10.1002/jnr.10365.

Figure legends

Figure 1. Morphological changes in hBM-MSC cultures during neural transdifferentiation. Time-lapse imaging revealed that, following neural induction, hBM-MSCs rapidly reshaped from a flat to a spherical morphology. Subsequently, we observed that hBM-MSC-derived round cells can preserve their spherical shape for several days (green arrows), change to that of neural-like cells through active neurite extension (red arrows) or revert back to the mesenchymal morphology (yellow arrows). Scale bar: 25 μm.

Figure 2. Morphological changes in dedifferentiated hBM-MSC. Time-lapse imaging showed the appearance (arrows), movement and disappearance (asterisk) of cellular protrusión from the surface of hBM-MSC-derived round cells. Scale bar: 25 μm.

Figure 3. Neuronal polarisation of dedifferentiated hBM-MSCs. Time-lapse imaging revealed the growth of new neurites from the body of round cells that which gradually adopted a complex morphology, acquiring dendrite-like (green arrows) and axon-like domains (yellow arrows). There was no observation of any transient cellular protrusión as hBM-MSC-derived round cells gradually acquired a neural-like morphology. Scale bar: 25 μm.

Figure 4. hBMSCs can repeatedly switch lineages. Time-lapse imaging showed that hBM-MSCs can also rapidly switch lineages without cell division. Mesenchymal morphology (green arrows); switching lineages (white arrows); dediffentiation morphology (red arrows); neural-like morphology (yellow arrows). Scale bar: 25 μm.

Figure 5. Nucleus remodelling occurs during neural transdifferentiation from hBM-MSCs. Time-lapse microscopy evidenced that nuclear remodelling occurred during neural transdifferentiation from histone H2B-GFP-expressing hBM-MSCs. Nuclei from hBM-MSC-derived round cells moved within the cell, adopting different morphologies, including finger shaped (red arrows) and kidney shaped (white arrows), and even forming lobed nuclei connected by nucleoplasmic bridges (yellow arrows). Scale bar: 25 μm.

Figure 6. Nuclear movement generated cellular protrusions that appeared and disappeared from the surface of hBM-MSC-derived round cells. Time-lapse microscopy revealed that the cell nucleus of histone H2B-GFP-expressing hBM-MSCs acquired a finger-like shape and moved within the cell, generating the transient cellular protrusions (arrows) on the surface of the hBM-MSC-derived round cells. Scale bar: 25 μm. PhC: Phase-contrast photomicrographs.

Figure 7. Binucleated hBM-MSCs can form with independence of any cell fusion events. Time-lapse microscopy revealed that the nuclei from histone H2B-GFP-expressing, dedifferentiated hBM-MSCs can move within the cell, forming lobed nuclei connected by nucleoplasmic bridges. The movement of the lobed nuclei also generated cellular transient protrusions from the surface of hBM-MSC-derived round cells. Scale bar: 25 μm. PhC: Phase-contrast photomicrographs.

Supplementary figures

Figure S1. Dedifferentiated hBM-MSC nuclei can switch their morphology and positioning. Time-lapse microscopy highlighted that the cell nucleus from histone H2B-GFP-expressing hBM-MSCs can switch its morphology while it is moving. Here, the nucleus acquired a finger-like shape before reorienting toward a peripheral position within the cell and acquiring a kidney-like shape. Subsequently, the cell nucleus began to move rapidly around the cell. Scale bar: 25 μm.

Figure S2. Mononucleated dedifferentiated hBM-MSCs position their nucleus at the front of the cell during migration. A) Time-lapse microscopy showed that kidney-shaped, histone H2B-GFP-expressing, dedifferentiated hBM-MSCs cells positioned their nucleus at the front of the cell during migration. **B)** In addition, finger-shaped, histone H2B-GFP-expressing, dedifferentiated hBM-MSCs also positioned their nuclei at the front of the cell during migration. Scale bar: 25 μm.

Figure S3. Dedifferentiated hBM-MSC with lobed nuclei position their nucleus at the front of the cell during migration. A) Time-lapse microscopy showed that histone H2B-GFP-expressing, dedifferentiated hBM-MSCs with lobed nuclei positioned their nucleus at the front of the cell during migration. **B)** Futhermore, histone H2B-GFP-

569 expressing, dedifferentiated hBM-MSCs with lobed nuclei positioned their largest lobe
570 at the front of the cell during migration. Scale bar: 25 μm.

571 **Figure S4. Nuclear morphology and positioning during neuronal polarisation of**
572 **dedifferentiated hBM-MSCs.** Time-lapse microscopy did not reveal any changes in
573 nuclear positioning or lobed nuclei formation as histone H2B-GFP-expressing, hBM-
574 MSC-derived round cells gradually acquired a neural-like morphology (asterisks). Scale
575 bar: 25 μm.

576 **Figure S5. Nuclear morphology when hBM-MSC-derived round cells**
577 **redifferentiate back to the mesenchymal fate. A)** Time-lapse microscopy revealed
578 that when histone H2B-GFP-expressing, dedifferentiated hBM-MSCs with a single
579 nucleus reverted back to the mesenchymal morphology (asterisk), the nuclei gradually
580 reverted back to their original ellipsoid shape. **B)** By contrast, when histone H2B-GFP-
581 expressing, dedifferentiated hBM-MSCs with lobed nuclei reverted back to the
582 mesenchymal morphology (asterisk), the lobed nuclei were maintained for hours. Scale
583 bar: 25 μm.

584 **Figure S6. hBM-MSCs exhibit unusual nuclear structures and chromatin-**
585 **containing bodies in the cellular cytoplasm during neural transdifferentiation. A)**
586 Confocal microscopy analysis showed that histone H2B-GFP-expressing hBM-MSCs
587 with a finger-shaped nucleus can also present chromatin-containing bodies in the
588 cellular cytoplasm. **B)** Histone H2B-GFP-expressing hBM-MSCs a kidney-shaped
589 nucleus can also exhibit chromatin-containing bodies in the cellular cytoplasm. **C)**
590 Histone H2B-GFP-expressing hBM-MSCs with a lobed nucleus connected by
591 nucleoplasmic bridges can also exhibit chromatin-containing bodies in the cellular
592 cytoplasm. **D)** We noted that histone H2B-GFP-expressing hBM-MSCs with chromatin-

containing bodies were connected to the main body of the nucleus by thin strands of nuclear material. **E)** Furthermore, histone H2B-GFP-expressing hBM-MSCs with chromatin-containing bodies moved away from or toward the main nuclei. **F)** Histone H2B-GFP-expressing hBM-MSCs with two lobed nuclei unconnected by any nucleoplasmic bridges with chromatin-containing bodies in the cellular cytoplasmwere also observed. Scale bar: 10 μm.

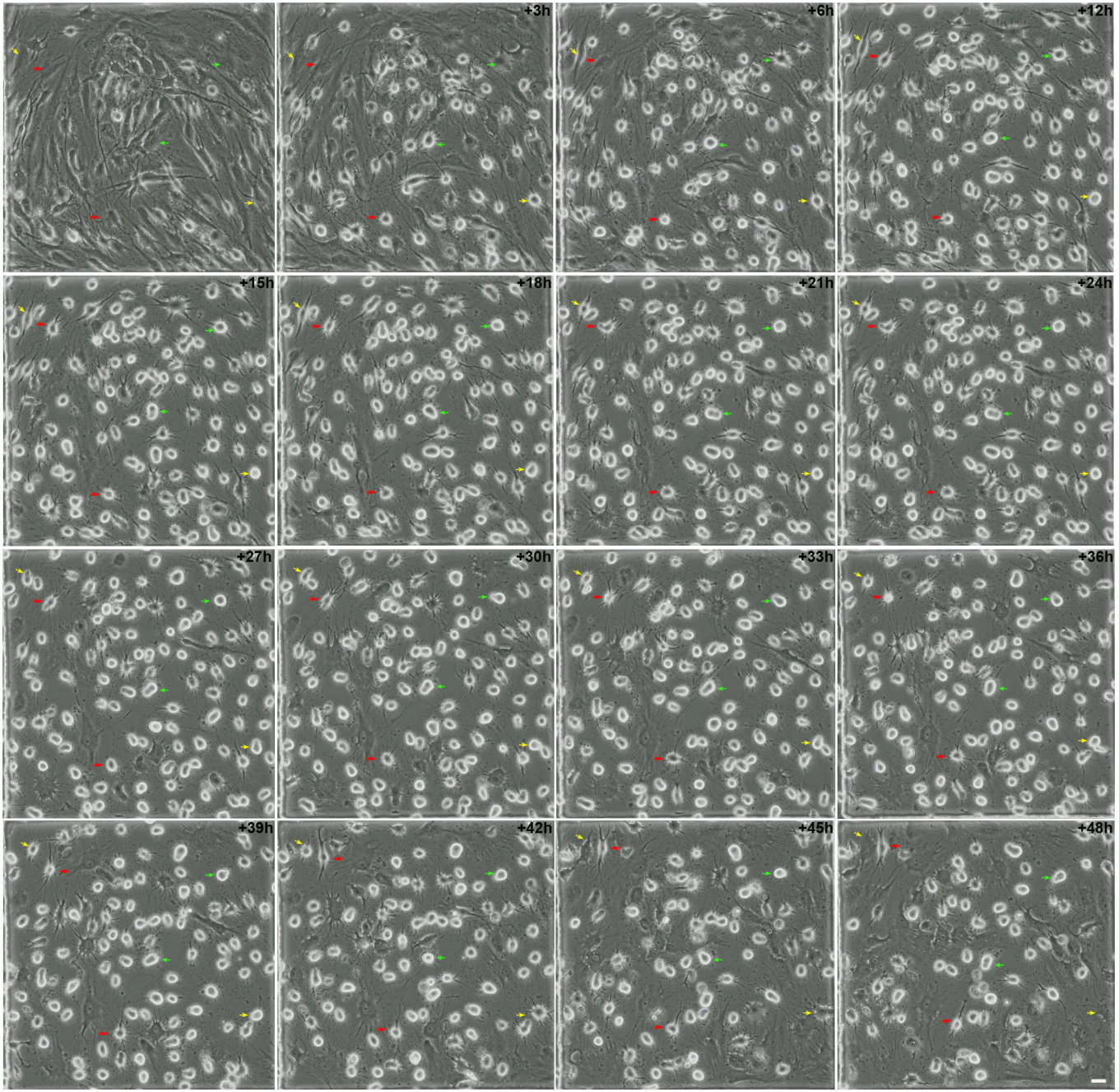

Figure 1

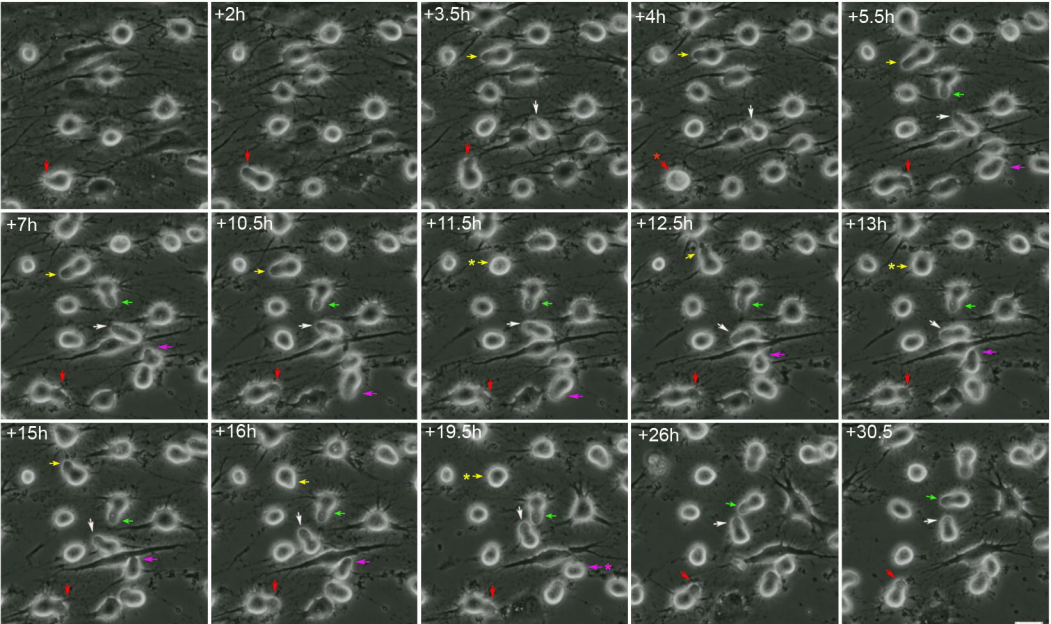

Figure 2


+0.5h
+1h
+1.5h
+2h
+2.5h
+3h
+3.5h
+4h
+4.5h
+5h
+5.5h
+6h
+6.5h
+7h
+7.5h
+8h
+8.5h
+9h
+9.5h
+10h
+10.5h
+11h
+11.5h
+12h
+12.5h
+13h
+13.5h
+14h
+14.5h
+15h
+15.5h
+16h
+16.5h
+17h
+17.5h
+18h
+18.5h
+19h
+19.5h
+20h
+20.5h
+21h
+21.5h
+22h
+22.5h
+23.5h
+24h
+24.5h

Figure 3

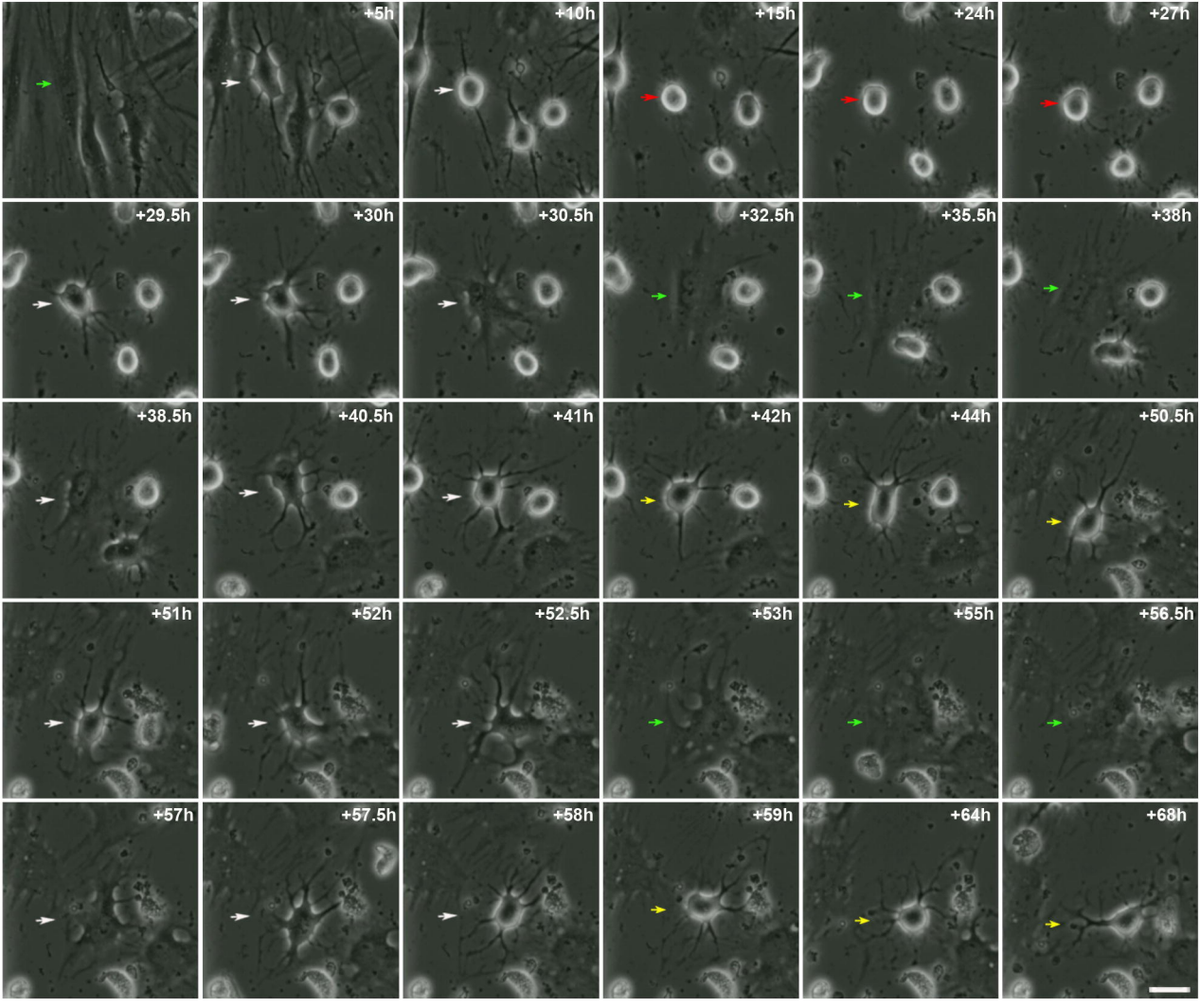
+5h
+10h
+15h
+24h
+27h
+29.5h
+30h
+30.5h
+32.5h
+35.5h
+38h
+38.5h
+40.5h
+41h
+42h
+44h
+50.5h
+51h
+52h
+52.5h
+53h
+55h
+56.5h
+57h
+57.5h
+58h
+59h
+64h
+68h

Figure 4

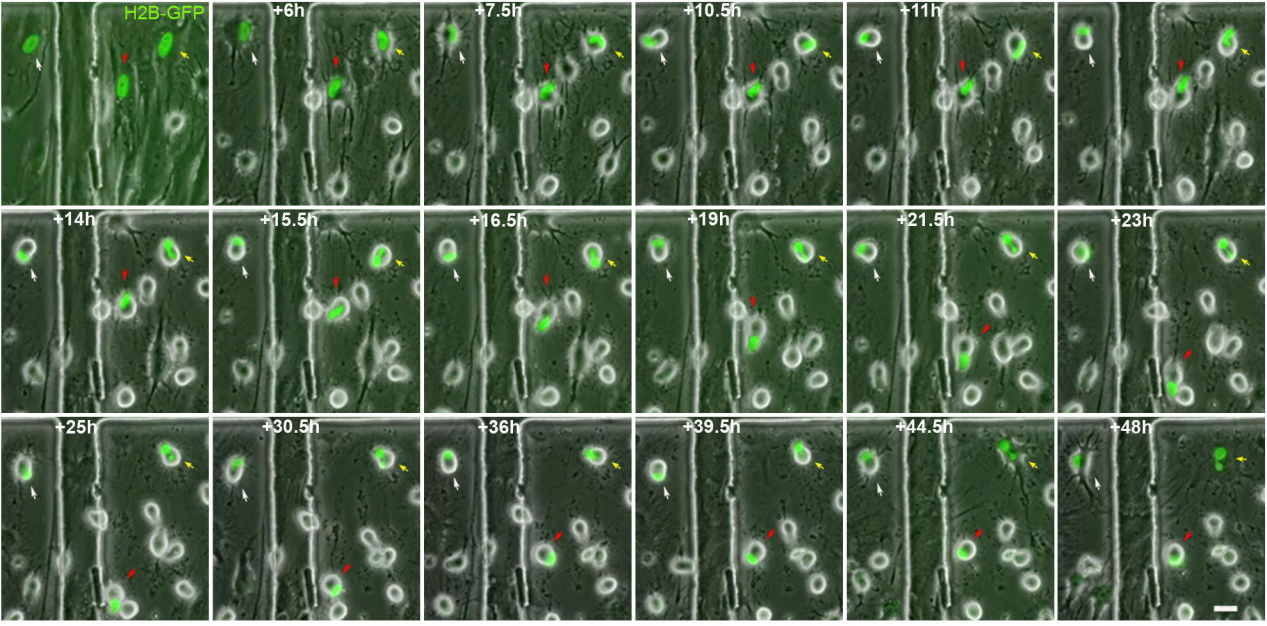
H2B-GFP
+6h
+7.5h
+10.5h
+11h
+14h
+15.5h
+16.5h
+19h
+21.5h
+23h
+25h
+30.5h
+36h
+39.5h
+44.5h
+48h

Figure 5

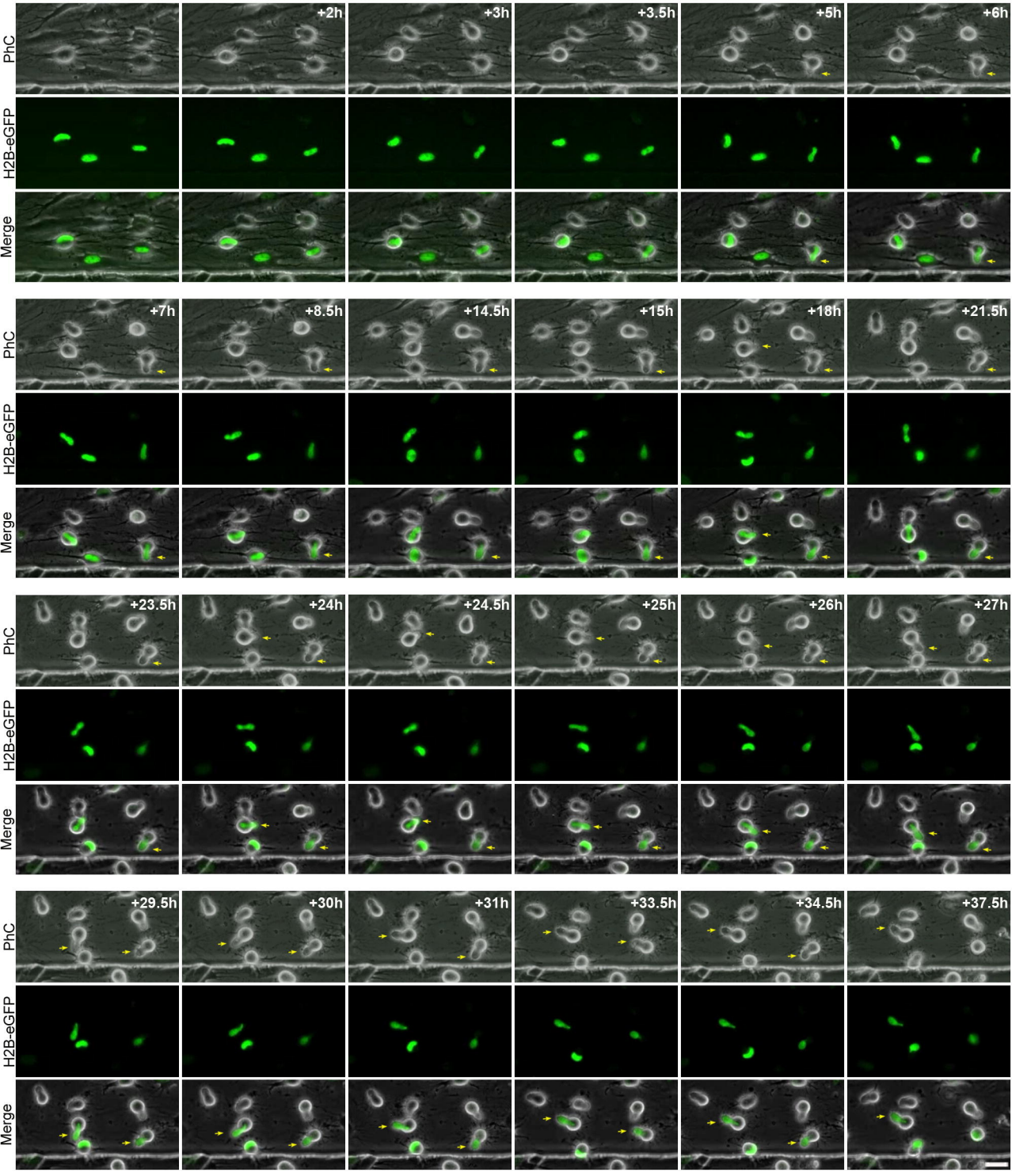
PhC
H2B-eGFP
Merge
+2h
+3h
+3.5h
+5h
+6h
+7h
+8.5h
+14.5h
+15h
+18h
+21.5h
+23.5h
+24h
+24.5h
+25h
+26h
+27h
+29.5h
+30h
+31h
+33.5h
+34.5h
+37.5h

Figure 6

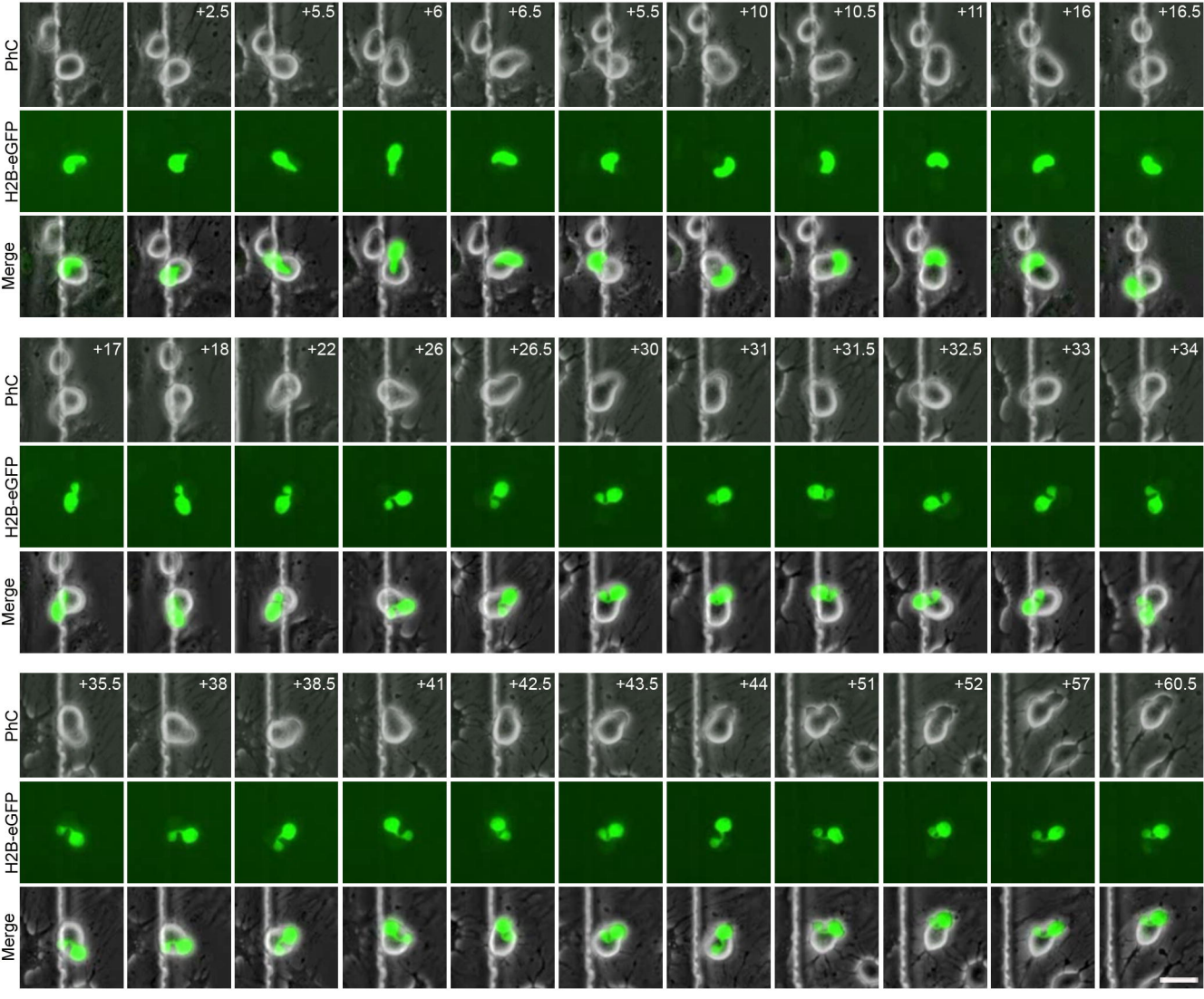
PhC
H2B-eGFP
Merge
+2.5
+5.5
+6
+6.5
+5.5
+10
+10.5
+11
+16
+16.5
+17
+18
+22
+26
+26.5
+30
+31
+31.5
+32.5
+33
+34
+35.5
+38
+38.5
+41
+42.5
+43.5
+44
+51
+52
+57
+60.5

Figure 7

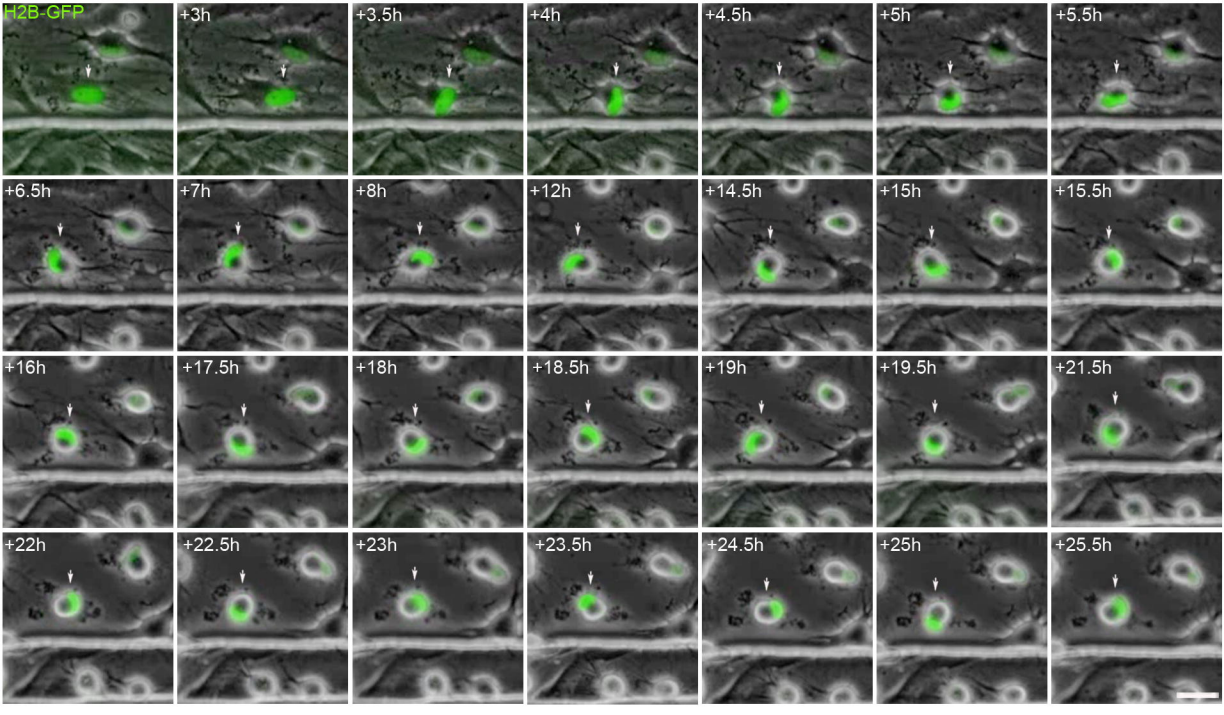
H2B-GFP
+3h
+3.5h
+4h
+4.5h
+5h
+5.5h
+6.5h
+7h
+8h
+12h
+14.5h
+15h
+15.5h
+16h
+17.5h
+18h
+18.5h
+19h
+19.5h
+21.5h
+22h
+22.5h
+23h
+23.5h
+24.5h
+25h
+25.5h

Figure S1

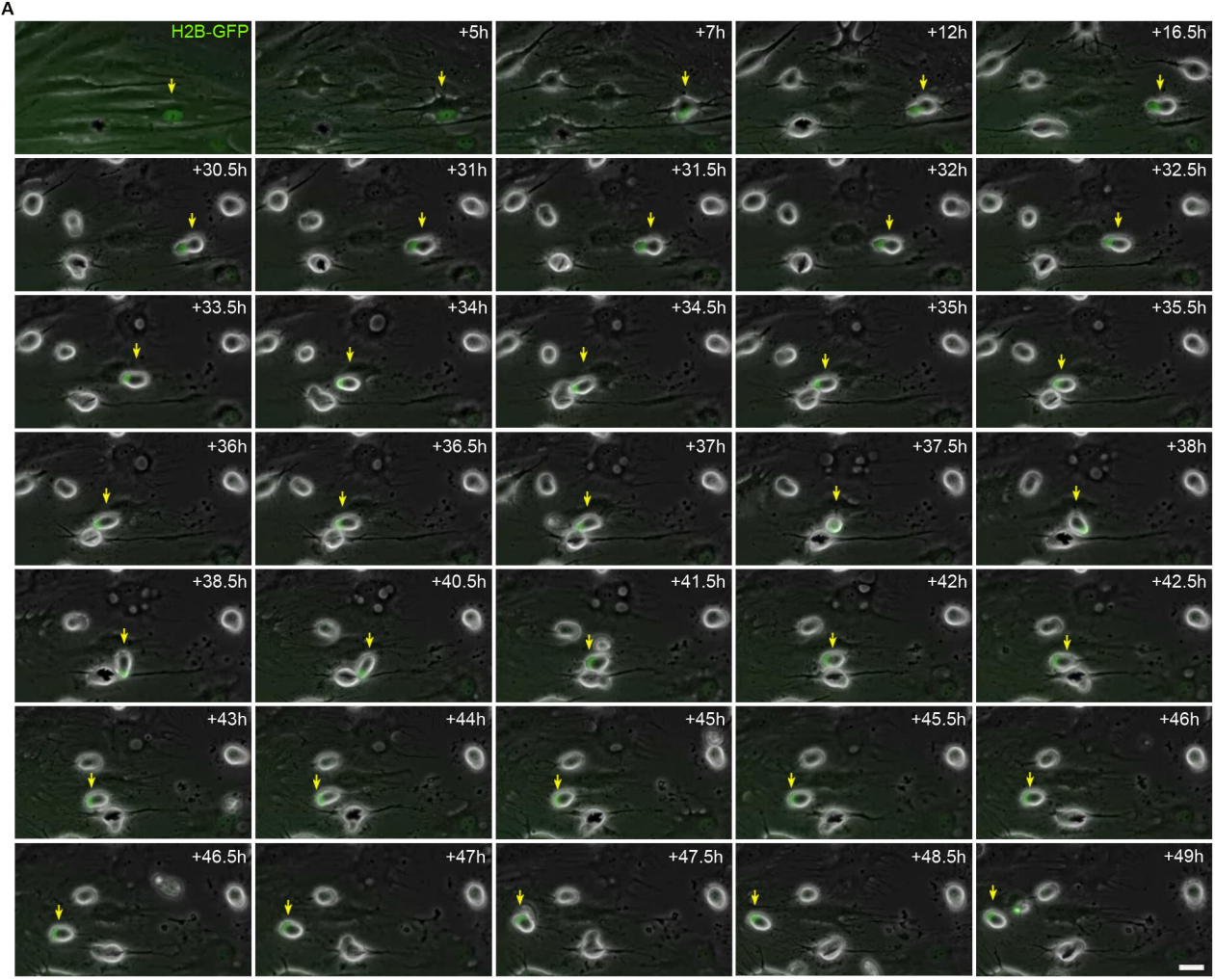
A
H2B-GFP
+5h
+7h
+12h
+16.5h
+30.5h
+31h
+31.5h
+32h
+32.5h
+33.5h
+34h
+34.5h
+35h
+35.5h
+36h
+36.5h
+37h
+37.5h
+38h
+38.5h
+40.5h
+41.5h
+42h
+42.5h
+43h
+44h
+45h
+45.5h
+46h
+46.5h
+47h
+47.5h
+48.5h
+49h

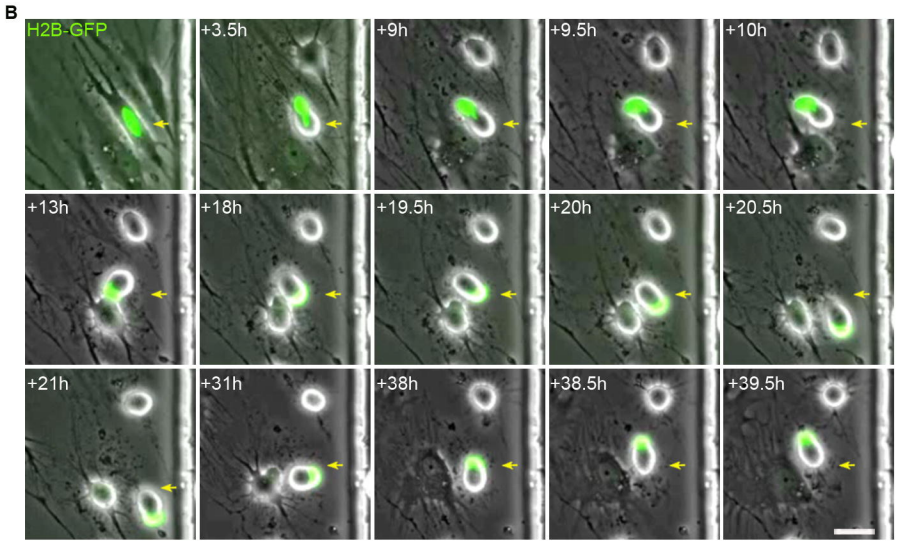
B
H2B-GFP
+3.5h
+9h
+9.5h
+10h
+13h
+18h
+19.5h
+20h
+20.5h
+21h
+31h
+38h
+38.5h
+39.5h

Figure S2

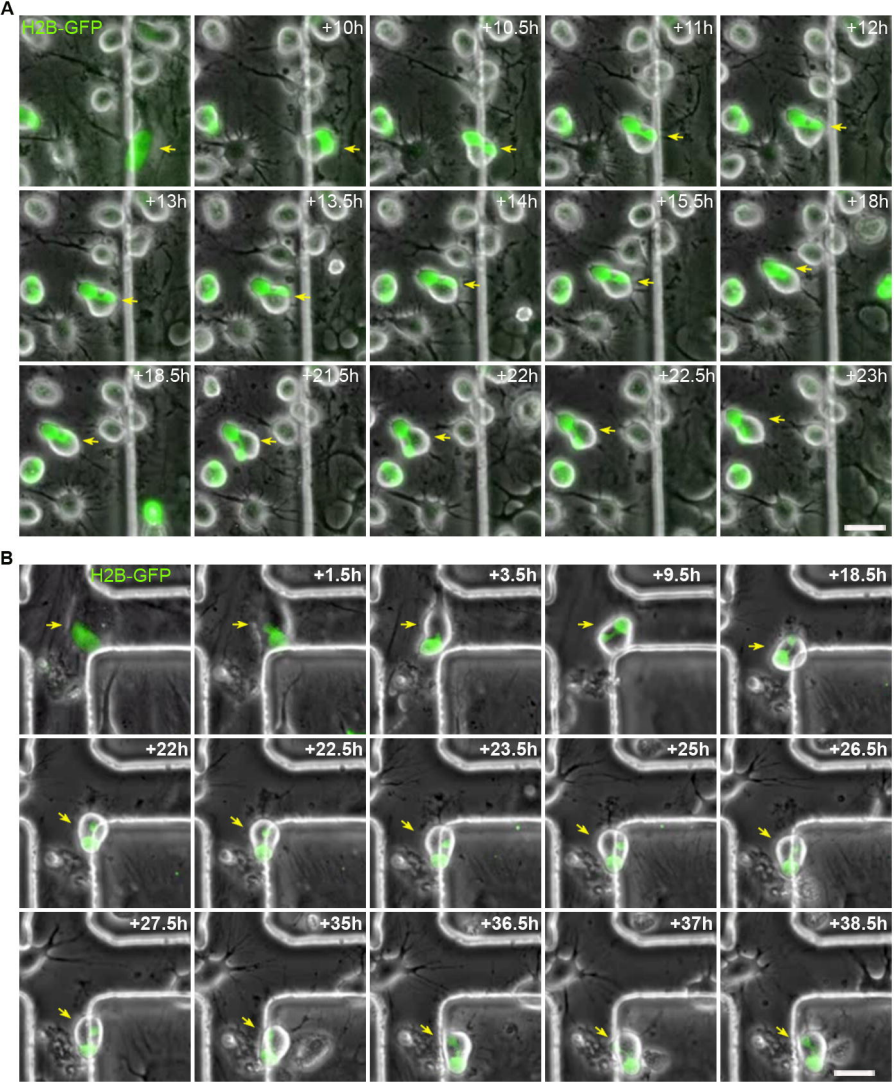
A
H2B-GFP
+10h
+10.5h
+11h
+12h
+13h
+13.5h
+14h
+15.5h
+18h
+18.5h
+21.5h
+22h
+22.5h
+23h
B
H2B-GFP
+1.5h
+3.5h
+9.5h
+18.5h
+22h
+22.5h
+23.5h
+25h
+26.5h
+27.5h
+35h
+36.5h
+37h
+38.5h

Figure S3

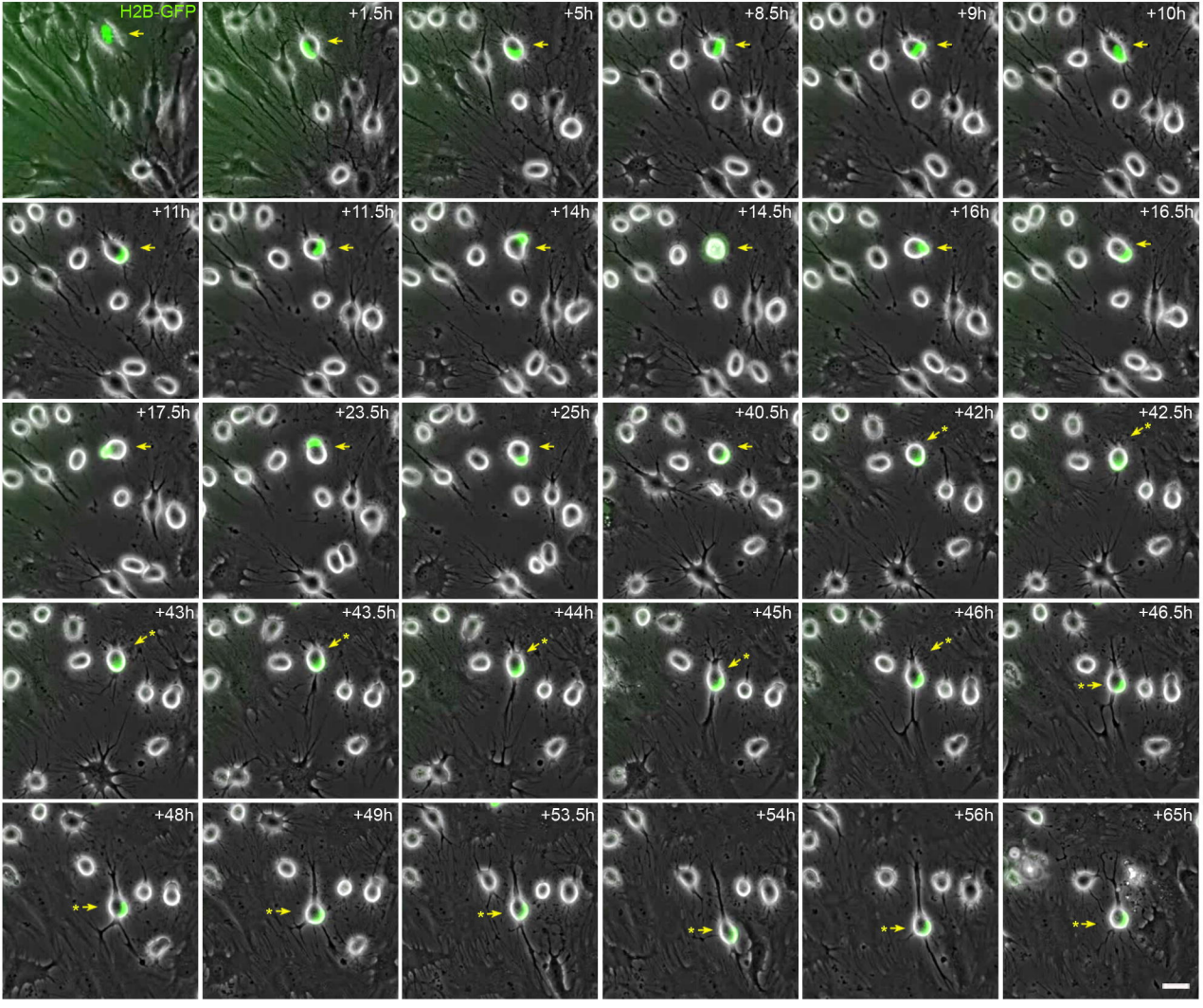
H2B-GFP
+1.5h
+5h
+8.5h
+9h
+10h
+11h
+11.5h
+14h
+14.5h
+16h
+16.5h
+17.5h
+23.5h
+25h
+40.5h
+42h
+42.5h
+43h
+43.5h
+44h
+45h
+46h
+46.5h
+48h
+49h
+53.5h
+54h
+56h
+65h

Figure S4

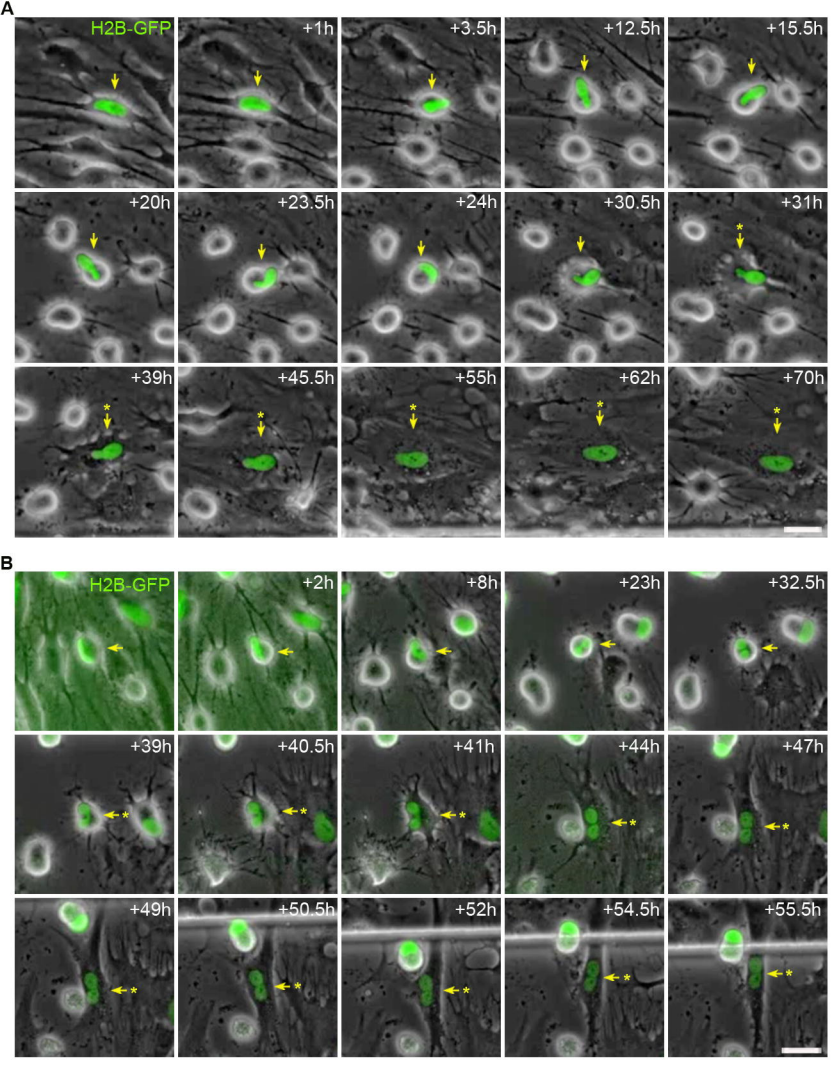
A
H2B-GFP
+1h
+3.5h
+12.5h
+15.5h
+20h
+23.5h
+24h
+30.5h
+31h
+39h
+45.5h
+55h
+62h
+70h
B
H2B-GFP
+2h
+8h
+23h
+32.5h
+39h
+40.5h
+41h
+44h
+47h
+49h
+50.5h
+52h
+54.5h
+55.5h

Figure S5

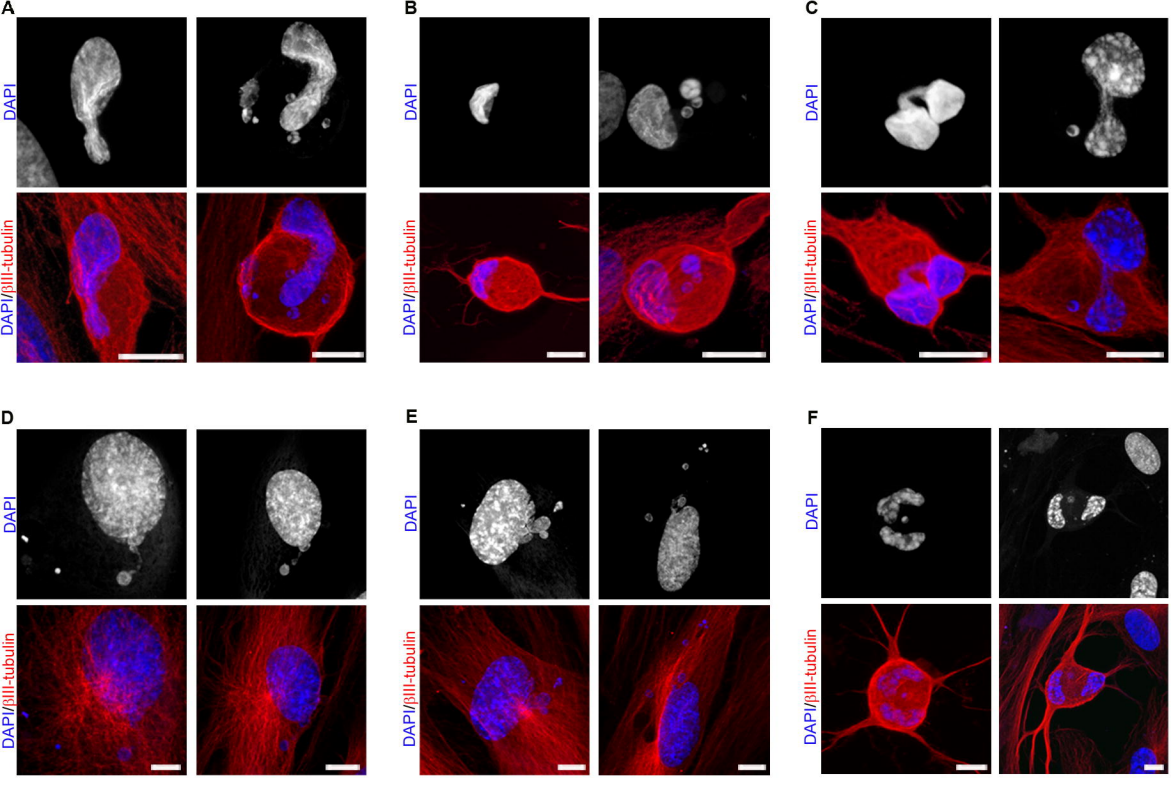

Figure S6